

Spatial and Temporal Temperature Homogenization in an Automotive Lithium-Ion Pouch Cell Battery Module



Markus Gepp, Vincent Lorentz, Martin März, Fanny Geffray, Elsa Guyon, and Fabrice Chopard

Abstract A battery system with a thermally optimized module design with regard to boundary conditions in automotive applications is developed. Measures for spatial and temporal temperature homogenization are realized. Highly thermal conductive pyrolytic graphite sheets as heat spreaders replace conventional metallic cooling sheets in a lightweight module design. Efficient space utilization with a novel phase change material for thermal peak-shaving enables benefits in thermal management and lifetime. Heat-conductive adhesives and elastomer-based gap filler sheets further reduce the thermal resistance and the rise in temperature. Measurements showed a maximum temperature difference between the cells of 4.3 K and a maximum thermal resistance between cells and coolant of 0.12 K/W. By integrating thermal solutions, the gravimetric and volumetric overhead was reduced by 25% and 10% compared to the state of the art.

Abbreviations

DCR	Direct current resistance
DOD	Depth of discharge
EIS	Electrochemical impedance spectroscopy
EOL	End of life
NMC	Lithium nickel manganese cobalt oxide
PCM	Phase change material
PGS	Pyrolytic graphite sheets
SEI	Solid electrolyte interface
SOC	State of charge
SOH	State of health

M. Gepp (✉) · V. Lorentz · M. März
Fraunhofer Institute for Integrated Systems and Device Technology, Erlangen, Germany
e-mail: markus.gepp@iisb.fraunhofer.de; vincent.lorentz@iisb.fraunhofer.de

F. Geffray · E. Guyon · F. Chopard
Hutchinson SA Centre de Recherche, Chalette-sur-Loing, France
e-mail: fabrice.chopard@hutchinson.com

1 Introduction

Specifications for battery systems in automotive applications demand cost-effective solutions with high power and energy densities. From a module designer's view, this restricts the volumetric and gravimetric overhead that is available for battery design and thermal management referred to as the cumulated cell's volume and weight.

Regarding the thermal management, automotive batteries face various and unsteady operation conditions, such as varying ambient conditions due to external heat sources or a wide range of mission profiles and fluctuations in ambient temperatures, placing high demands on thermal management. Furthermore, thermal stress and overheating caused by peak loads need to be limited by derating strategies.

Another specification is a sufficient battery service life, which is directly connected to temperature-related cycle and calendrical aging. High temperatures—according to Arrhenius law—as well as low temperatures, lead to accelerated aging mechanisms and degradation of the cell. On module level, temperature differences between parallel- and series-connected cells or local hot spots have adverse impact on the system service life.

In order to meet the requirements and challenges, a battery module with advanced thermal management is designed. Temperature-related aging and performance is considered for a pouch cell module in NMC/graphite chemistry, to derive the potential and the requirements for the thermal management such as temperature homogenization both spatial and temporal. The module design comprises a thermal separation of the cells for temperature homogenization and the use of flexible highly thermal conductive graphite sheets to dissipate heat. A gap filler material is developed and a highly thermal conductive glue is used to reduce contact resistances, while temperature peaks are compensated with a new developed phase change material with an enhanced thermal conductivity.

A variety of thermal management approaches and concepts based on PCM and graphite sheets is available, evaluated on simulation level or on test bench with simplified setups [1–3]. Aim of this investigation is to achieve application-oriented and comparable results, with a detailed constructed module including the integrated thermal management, and to meet the essential requirement of a low design space overhead. An assessment of temperature-related aging with regard to the selected cell type and chemistry enables an evaluation of the thermal management measures.

2 Temperature-Dependent Aging and Performance

2.1 Aging Phenomena

General statements concerning battery aging, caused by side reactions in the battery, are only possible to a limited extent due to a large variety of Li ion chemistries [4]. In [5] several studies on temperature-dependent aging with different chemistries

are reviewed. Aging phenomena are identified in capacity decay and power fading, i.e., rise of the internal impedance, resulting from various processes and their interactions [6].

Capacity decay is analyzed in $dV/dSOC$ measurements, whereas voltage peaks are representing transitions between voltage plateaus of the negative electrode. These peaks are shifted or vanished over cycling due to aging-related loss of active material or lithium [7].

The rise of impedance is measured with electrochemical impedance spectroscopy (EIS), assuming an equivalent model with capacitor-resistor elements. The electrode polarization resistance is connected to the charge transfer resistance at low frequency while high-frequency resistances are associated with SEI layer growth. The ohmic resistance results from the electrolyte, separator, and current collectors [8].

The aging process can be separated in mechanisms at the cathode and anode during cycling and storage, depending on SOC, DOD, currents, and temperature level [6]. In the following, the cycle aging is described for NMC/graphite cells.

2.2 Aging Mechanisms and Their Temperature Dependency

A good overview of aging mechanisms is given in [6, 9], and [8]. The major source for aging at the negative graphite electrode is considered to be connected to the electrode-electrolyte interface SEI [4, 8]. The anode voltage operates outside the electrochemical stability related to the organic solvent. Electrolyte decomposition, electrode corrosion, and irreversible consumption of lithium result in capacity fade and impedance rise but also lead to the formation of the protective and passivating SEI. This effect is mainly dependent on electrolyte and therefore increased for elevated temperatures, accelerating the reaction kinetics. Due to diffusing particles, the SEI growth with morphology changes and reformation is ongoing after its initial formation. SEI components are converted to resistive inorganic products with lower ionic conductivity, increasing the internal resistance of the battery.

When the battery is cycled, the intercalation of lithium ions and volume changes mechanically stress the electrode and result in particle cracking, gas evolution, and graphite exfoliation. The carbon structure seems to be destroyed by voltage-level transitions at high depth of discharge (DOD), leading to capacity fade [7]. The mechanical stability of the electrode is also worsened due to the continuous decomposition of the binder at high SOC and high temperatures.

Both electrodes are deteriorated by power fade due to current collector corrosion and SEI growth, decreasing accessible contact surface area and porosity.

At low temperatures, the intercalation potential of the carbonaceous anode is close to the potential of lithium metal [10]. Slow lithium kinetics at high currents lead to local and inhomogeneous lithium plating, where the electrolyte is decomposed by metallic lithium, resulting in loss of lithium and electrolyte (capacity and power fade) [11]. The functional capability of the battery is also

affected by a false capacity reduction due to an increased internal resistance and polarization effect at low temperatures. This false reduction of usable capacity can still be discharged at low currents [12].

At the positive electrode, the major source for aging is considered to be capacity fade through structural changes such as phase transitions and disordering in the bulk material and SEI layer formation at high temperatures [6, 8]. In addition, at high temperatures chemical decomposition and dissolution of the cathode leads to metal transition to anode resulting in anode SEI layer growth.

2.3 Impact on Cycle Life for Elevated Temperatures

The state of health (SOH) is a predefined measure of aging depending on cycle life and calendar life; its indicators are capacity retention and impedance rise. According to [13], the definition of end of life (EOL) for batteries is application specific. EOL is reached at 80% of the nominal capacity rated by the manufacturer or at a doubled actual internal resistance. While a capacity reduction is generally definable, the frequency-dependent impedance needs to be regarded as application specific. For power applications, the direct current resistance (DCR) is typically used [14]. The DCR, which is the sum of ohmic and polarization resistance, provides a sufficient basis for the following estimation, but it cannot completely describe the dynamic behavior of the battery.

To estimate the impact of temperature-dependent aging and performance, a search on aging tests of commercial large format pouch cells with NMC/graphite chemistry is conducted. In [8] the necessary data for temperature-dependent cycle life, according to the above-described EOL conditions, can be extracted. The DCR doubles at cycle 1600 at room temperature, cycle 1200 at 45 °C, and cycle 300 at 65 °C while the capacity limit of 80% is reached after 2600 cycles at room temperature, 2000 cycles at 45 °C, and 800 cycles at 65 °C. It can be concluded, considering both EOL limits, that cycle life is reduced by about 25% for elevated temperatures and 75% for high temperatures.

On module level, temperature gradients between the cells are regarded. Simply said, not considering any internal or cooling structure, a temperature distribution over the module with a hot spot in the middle is expected. The temperature rise is caused by the heat generation of the cells and is in linear relationship to the current, because of a quadratic dependence of power losses and an exponentially decreasing internal resistance [15, 16]. Consequently, higher currents or internal resistances, e.g., at low ambient temperatures, result in higher temperature gradients. For example, a temperature difference of 6 K in a non-homogenized pouch module after a 3C discharge at 25 °C is given [17]. In [18] and [19] similar values were determined for modules with different cell types and chemistries.

The temperature gradients lead to different aging rates of the single cells depending on their position in the module. For example, for parallel connected cells, a linear dependency between capacity loss and temperature difference was

found in [20] and [21]. By interpolation of temperature-related cycle life according to the specified EOL limits and considering a typical temperature difference of 6 K in a module, lifetime of the single cells differs roughly 5% for moderate, 8% for elevated, and 20% for high temperatures.

To quantify the impact on module lifetime, additional module-specific information regarding the temperature distribution and, due to the temperature dependency of the maximum temperature gradient, typical temperature profiles while in operation are necessary. Besides, voltage balancing and derating strategies compensate the impact of diverging SOHs on the system lifetime.

Considering the temperature-dependent aging mechanisms and their impact on service life enables to draw the following conclusions:

- The aging rate at the lower and upper limits of the temperature range is significantly increased.
- Temperature differences in the module arise during cycling depending on electrical and thermal boundary conditions.
- Temperature differences lead to diverging states of health of the cells, reducing the system lifetime.
- The impact of temperature differences on state of health is increased for higher temperatures.

These conclusions are addressed by measures of temporal and spatial homogenization with the following approach:

3 Module Concept and Construction

3.1 Description of the Concept and Construction

The module structure is described in Fig. 1, with a section view seen from the top side.

Casted PCM parts are located on both lateral sides of the cells and align them within the vacuum molded plastic frames. Soft cellular silicone foams provide initial pressure and swelling compensation. As heat spreaders, PGS graphite foils are



Fig. 1 Concept of the module in cross-section view

directly adhered to the cell surfaces and connect them with PCM and metal profiles by thermal conductive glue. Milled aluminum profiles are designed as mold inlays for the frames and provide mechanical stability and a thermal connection to the cooling plates. Commercial liquid cooling plates are combined with conformable gap filler sheets to compensate geometrical production-related tolerances and thus eliminate air gaps for a reduced thermal resistance. All cells are connected in series by ultrasonic welding.

As previously described, the design of the prototype module is restricted to production processes, which are economical for low quantities. For example, vacuum casting instead of injection molding demands higher wall thicknesses. Nevertheless, the focus is on a lightweight construction to reduce gravimetric and volumetric design overhead. Figure 2 shows the assembled prototype.

3.2 Integration of Advanced Thermal Material Solutions

The thermal concept of the battery module was developed in close cooperation with industrial partners, supporting the integration of thermal material solutions. The integrated components are shown in Fig. 3.

Fig. 2 Battery module prototype



Fig. 3 Frame including PGS foil and PCM inlays



3.2.1 Panasonic Pyrolytic Graphite Sheets (PGS)

The synthetic pyrolytic graphite sheets with a thickness of $70\ \mu\text{m}$ have an in-plane thermal conductivity of $1000\ \text{W}/(\text{m K})$ and provide flexibility and a low minimal bending radius with high bending cycle stability. The material is used as a heat spreader between cells, frames, and PCM inlays. With its flexibility PGS can be directly adhered to the pouch cell and also compensates relative movements due to cell swelling with relief folds. The high thermal conductivity together with the low thermal contact resistance provides similar properties as metallic cooling sheets.

3.2.2 Hutchinson PCM PCsMart[®]

The PCsMart[®] is an elastomer-based smart phase change material, which stores latent heat during its melting and releases it during its solidification. It has a micro-encapsulated structure to maintain its solid state while melting. Two functions are aimed to be fulfilled in the battery system:

First is safety; overheating and thermal runaway have to be avoided. The PCsMart[®] is in thermal contact with the graphite sheets and cell edges and tabs to absorb the dissipated heat and store as latent heat. It provides a thermal buffer to the upper temperature limit. The velocity of the storage phase is improved by decreasing the thermal resistance of the PCM material with additives. The PCsMart[®] product has an increased thermal conductivity ($1.5\ \text{W}/(\text{m K})$) compared to common pure PCMs.

Its second function is to avoid accelerated aging at higher temperatures and extend lifetime. The variety of PCMs actually presents a wide range of melting temperature ranges whose width and peak depend on its chemical nature and the heat flow rate. Therefore the type of PCM material formula is adapted to this application. Regarding the battery cell NMC chemistry and its operation temperature, the optimum in order to fulfill both functions is a melting range from 35 to 55 °C.

3.2.3 Hutchinson Gap Filler Material

Hutchinson gap filler material is a thermally conductive interface pad. It compensates the geometrical production-related tolerance of the frames because of its mechanical properties. Consequently, it allows reducing the thermal contact resistance due to air gaps and thus optimizing heat transfer. The gap filler sheet with a high through-plane conductivity of 4 W/(m K) leads to a preferential thermal path. It helps to homogeneously distribute heat on the cooling plate and thus improve the efficiency of the latter. With its low density (1 g/cm³) and its UL 94 V-0 classification, Hutchinson gap filler is suitable in automotive applications.

3.2.4 Polytec PT Thermal Conductive Adhesive

The pasty adhesive has an improved thermal conductivity of 2 W/(m K) due to non-abrasive additives. It provides mechanical flexibility and cures at room temperature. The adhesive has a good adhesion on metal and plastics and is used to thermally connect all components along the thermal path in the battery module, e.g., PGS, PCM inlays, frames, and gap filler.

3.3 *Temporal and Spatial Temperature Homogenization*

Temporal and spatial temperature homogenization are addressed with the following measures (beginning with temporal temperature homogenization):

- Phase change material (PCM) reduces the overall temperature rise due to its additional thermal mass. In this concept, the integrated PCM mass has one-third of the specific heat (J/K) referred to as specific heat of the cells.
- The PCM is also used for thermal peak-shaving by adjusting the phase change of the material to the upper temperature range of the cells. The enthalpy consumed for the phase change corresponds to the enthalpy for heating up the PCM and cells by 9 K.
- By thermally connecting the PCM in parallel to the heat path, an adverse impact on the thermal resistance and on the temperature rise by PCM is avoided.

Spatial temperature homogenization is achieved by the reduction of the thermal resistances by:

- Development of new conformable and high through-plane conducting gap filler sheets to reduce contact resistance
- Thin and flexible highly thermal conductive PGS for heat spreading connected with a heat-conducting adhesive

Internal constructive asymmetries are avoided by foams, presenting a thermal barrier between the cells. This prevents the formation of a spatial temperature gradient and different temperature-induced aging rates.

4 Experimental Setup and Test Procedure

The experimental setup is described in Figs. 4 and 5. The battery module within a temperature chamber is cooled by a thermostat. Inlet and outlet temperatures as well as the flow rate of the coolant are measured. A source and sink provide the electrical load cycle; voltage and temperature at the hot spot of all cells are logged.

Fig. 4 Schematic test setup

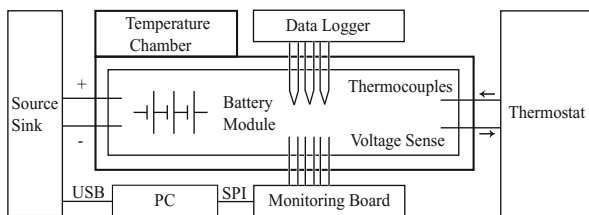


Fig. 5 Experimental setup



5 Results and Discussion

The prototype is assessed with regard to three criteria. Spatial homogenization is shown by measuring the maximum temperature difference between the cells at a test cycle. Temporal homogenization is evaluated by the maximum thermal resistance that determines the rise in temperature referred to as the dissipated heat. Third, the overhead in weight and volume is specified, making the mechanical concept comparable.

5.1 Spatial Temperature Homogenization

As test cycle, 50 A (2C) charge current with 10 A cutoff at 48 V and 130 A (5C) discharge current with cutoff at 35 V are applied (Fig. 6). Initial temperature, ambient temperature, and coolant temperature are set to 20 °C. The coolant is a water-glycol mixture with a flow rate of 3.7 L/min.

The temperatures of the single cells are measured and the arithmetic average is plotted in Fig. 7. A stationary state with a maximum temperature of 45 °C is reached after the second discharge cycle at 45 min. The rise in temperature in stationary state is 12 °C.

In Fig. 8, the maximum temperature difference between the hottest and coldest cell is plotted with a peak of 4.3 °C. The distribution of temperature is described as having a hot spot at the middle cells while the outer cells are colder. Due to warming of the fluid, the distribution is slightly shifted between coolant inlet and

Fig. 6 Electrical load cycle

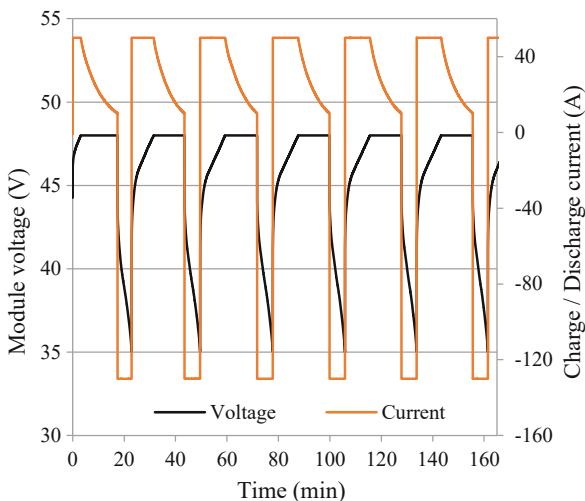


Fig. 7 Averaged temperature of the cells in module

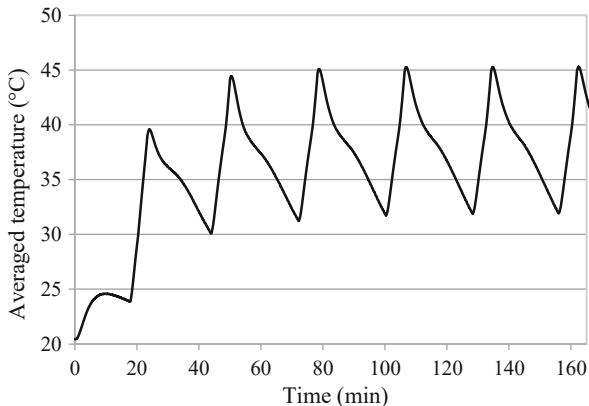
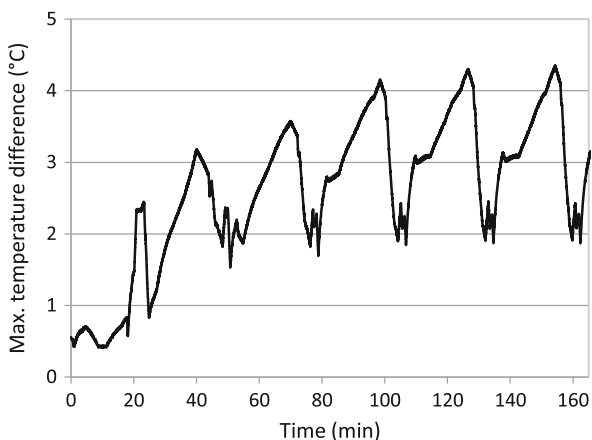


Fig. 8 Maximum temperature difference between hottest and coldest cell in module

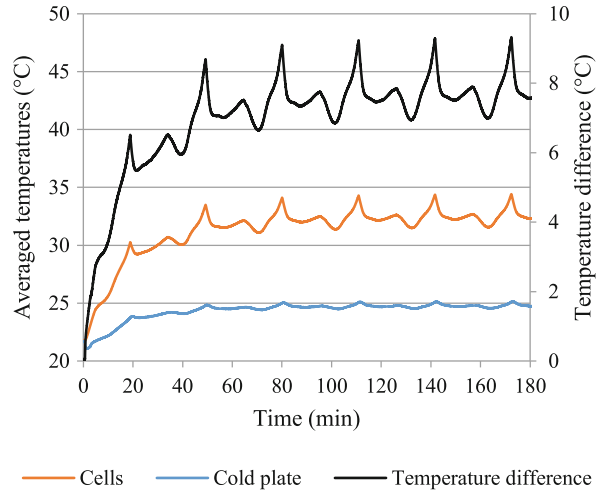


outlet of the cold plates. A measurement with similar conditions is conducted in [17] with a maximum temperature difference of 6 °C.

5.2 Maximum Thermal Resistance

The liquid-cooled module within the insulated temperature chamber is continuously cycled with 2C/2C charge/discharge current rates to apply roughly constant heat dissipation until stationary state is reached. The temperatures of the cells and the cold plates are measured and averaged, resulting in a maximum temperature difference of 8 °C in stationary state (Fig. 9). The extracted heat of 69 W is calculated by the coolant flow rate, its temperature rise, and the specific heat capacity of the water-glycol mixture. A reduced flow rate leads to higher temperature rise of the coolant

Fig. 9 Average mean temperatures of cells and cold plates



and improves the measurement accuracy. As result, a maximum thermal resistance between the averaged cell temperature and coolant of 0.12 K/W is determined.

5.3 Overhead Evaluation and Specifications

The gravimetric and volumetric overhead referred to as the cell's weight and volume is presented in Table 1. As reference, the Opel Ampera battery module with similar pouch cells from LG Chem is chosen. The frames concept using thin and light graphite sheets as heat spreaders reduces the overhead in weight by 25% and the overhead in volume by 10%. This also includes the PCM with an overall sensitive heat of 1.85 kJ/K and a latent heat of 70 kJ/K providing benefits in thermal management.

Finally, it should be remarked that mechanical safety measures besides non-flammability, e.g., measures against mechanical deformation in case of incidents, would require additional overhead, which was not the focus of this study.

6 Conclusion

A battery module is designed, assembled, and evaluated in order to demonstrate spatial and temporal temperature homogenization. Conventional aluminum cooling sheets are replaced by thin and light graphite foils. Novel elastomer-based gap filler pads as well as casted compressible elastomer-based PCM inlays are developed and integrated in the system. The thermal conductivity of the materials is enhanced by

Table 1 Mechanical, electrical, and thermal specifications

Specifications	Characteristics
Max. dimensions L × W × H (mm ³)	174.3 × 185.5 × 243.7
Module weight (kg)	11.15
Module volume (L)	7.88
Gravimetric overhead	40% (25% less than state of the art ^a)
Volumetric overhead	65% (10% less than state of the art ^a)
Configuration	12s1p
Nominal capacity (Ah)	25.9
Nominal voltage (V)	44.4
Max continuous current rate	6C
Temperature range (°C)	−30 ... +45
Conductivity PGS (W/(m K))	1000
Conductivity gap filler (W/(m K))	4 (through-plane)
Conductivity glue (W/(m K))	2 ± 0.2
Conductivity PCM (W/(m K))	1.5 (ASTM D5930-9)
Sensitive heat of incl. PCM (kJ/K)	1.85
Sensitive heat of incl. cells (kJ/K)	5.65
Latent heat of incl. PCM (kJ)	70
Melting range PCM (°C)	40 (35 ... 55)

^aCompared to Opel Ampera battery module, LG Chem pouch cells, liquid cooled, market launch 2012

additives and conductive glue. As result, the measurements showed a maximum temperature difference between the cells of 4.3 °C in a continuous cycle with maximum discharge current, a maximum thermal resistance of 0.12 K/W on module level, and a reduced gravimetric (−25%) and volumetric overhead (−10%) compared to the state of the art.

Acknowledgments The research leading to these results has received funding from the European Union’s Seventh Framework Programme for Research, Technological Development and Demonstration under grant agreement no. 608770 (“eDAS”).

The research leading to these results has also received funding from European Union’s Horizon2020 Programme for Research and Innovation under grant agreement no. 770019 (“GHOST”).

The authors acknowledge the Panasonic Device Solution Business Division for the supply of PGS and their technical support and collaboration.

The authors also acknowledge the Polytec PT GmbH for the supply of thermal conductive adhesives and their technical support and collaboration.

References

1. P. Goli, S. Legedza, A. Dhar, R. Salgado, J. Renteria, A.A. Balandin, Graphene-enhanced hybrid phase change materials for thermal management of Li-ion batteries. *J. Power Sources* **248**, 37–43 (2014)
2. N. Javani, I. Dincer, G.F. Naterer, G.L. Rohrauer, Modeling of passive thermal management for electric vehicle battery packs with PCM between cells. *Appl. Therm. Eng.* **73**, 307–316 (2014)
3. W.Q. Li, Z.G. Qu, Y.L. He, Y.B. Tao, Experimental study of a passive thermal management system for high-powered lithium ion batteries using porous metal foam saturated with phase change materials. *J. Power Sources* **255**, 9–15 (2014)
4. M. Broussely, P. Biensan, F. Bonhomme, P. Blanchard, S. Herreyre, K. Nechev, R.J. Staniewicz, Main aging mechanisms in Li ion batteries. *J. Power Sources* **146**, 90–96 (2005)
5. T.M. Bandhauer, S. Garimella, T.F. Fuller, A critical review of thermal issues in lithium-ion batteries. *J. Electrochem. Soc.* **158**, R1–R25 (2011)
6. J. Vetter, P. Novák, M.R. Wagner, C. Veit, K.-C. Möller, J.O. Besenhard, M. Winter, M. Wohlfahrt-Mehrens, C. Vogler, A. Hammouche, Ageing mechanisms in lithium-ion batteries. *J. Power Sources* **147**, 269–281 (2005)
7. M. Ecker, N. Nieto, S. Käbitz, J. Schmalstieg, H. Blanke, A. Warnecke, D.U. Sauer, Calendar and cycle life study of Li(NiMnCo)O₂-based 18650 lithium-ion batteries. *J. Power Sources* **248**, 839–851 (2014)
8. K. Jalkanen, J. Karppinen, L. Skogström, T. Laurial, M. Nisula, K. Vuorilehto, Cycle aging of commercial NMC/graphite pouch cells at different temperatures. *J. Appl. Energy* **154**, 160–172 (2015)
9. F. Leng, C.M. Tan, M. Pecht, Effect of temperature on the aging rate of li ion battery operating above room temperature. *Sci. Rep.* **5**, 12967 (2015)
10. J. Jaguemont, L. Boulon, P. Venet, Y. Dubé, A. Sari, Low temperature aging tests for lithium-ion batteries, in *IEEE International Symposium for Industrial Electronics*, (IEEE, Piscataway, NJ, 2015)
11. D. Burow, K. Sergeeva, S. Calles, K. Schorb, A. Börger, C. Roth, P. Heitjans, Inhomogeneous degradation of graphite anodes in automotive lithium batteries under low-temperature pulse cycling conditions. *J. Power Sources* **307**, 806–814 (2016)
12. X. Gong, C.C. Mi, Temperature-dependent performance of lithium ion batteries in electric vehicles, in *IEEE Applied Power Electronics Conference and Exposition, March*, (IEEE, Piscataway, NJ, 2015)
13. B. Scrosati, J. Garche, W. Tillmetz, *Advances in Battery Technologies for Electric Vehicles*, Woodhead Publishing Series in Energy Number 80 (Elsevier Ltd., Amsterdam, 2015)
14. W. Waag, S. Käbitz, D.U. Sauer, Experimental investigation of the lithium-ion battery impedance characteristic at various conditions and aging states and its influence on the application. *J. Appl. Energy* **102**, 885–897 (2013)
15. J. Shim, R. Kostecki, T. Richardson, X. Song, K.A. Striebel, Electrochemical analysis for cycle performance and capacity fading of a lithium-ion battery cycled at elevated temperature. *J. Power Sources* **112**, 222–230 (2002)
16. T. Waldmann, G. Bisle, B.I. Hogg, S. Stumpp, M.A. Danzer, M. Kasper, P. Axmann, M. Wohlfahrt-Mehrens, Influence of cell design on temperatures and temperature gradients in lithium-ion cells: an in operando study. *J. Electrochem. Soc.* **162**, A921–A927 (2015)
17. C. Veth, D. Dragicevic, C. Merten, Thermal characterizations of a large-format lithium ion cell focused on high current discharges. *J. Power Sources* **267**, 760–769 (2014)
18. M. Gepp, R. Filimon, S. Koffel, V.R.H. Lorentz, M. März, Advanced thermal management for temperature homogenization in high-power lithium-ion battery systems based on prismatic cells, in *IEEE International Symposium for Industrial Electronics*, (IEEE, Piscataway, NJ, 2015)

19. S. Paul, C. Diegelmann, H. Kabza, W. Tillmetz, Analysis of ageing inhomogeneities in lithium-ion battery systems. *J. Power Sources* **239**, 642–650 (2013)
20. N. Yang, X. Zhang, B. Shang, G. Li, Unbalanced discharging an aging due to temperature differences among the cells in a lithium-ion battery pack with parallel combination. *J. Power Sources* **306**, 733–741 (2016)
21. T. Bruen, J. Marco, Modelling and experimental evaluation of parallel connected lithium ion cells for an electric vehicle battery system. *J. Power Sources* **310**, 91–101 (2016)